

# Simulation of calcium waves in ascidian eggs: insights into the origin of the pacemaker sites and the possible nature of the sperm factor

Geneviève Dupont<sup>1,\*</sup> and Rémi Dumollard<sup>2</sup>

<sup>1</sup>Unité de Chronobiologie Théorique, Université Libre de Bruxelles, Faculté des Sciences CP231, Boulevard du Triomphe, Brussels 1050, Belgium

<sup>2</sup>Department of Physiology, University College London, Gower Street, London, WC1E 6BT, UK

\*Author for correspondence (e-mail: gdupont@ulb.ac.be)

Accepted 21 April 2004

Journal of Cell Science 117, 4313-4323 Published by The Company of Biologists 2004

doi:10.1242/jcs.01278

## Summary

Fertilization triggers repetitive waves of cytosolic  $\text{Ca}^{2+}$  in the egg of many species. The mechanism involved in the generation of  $\text{Ca}^{2+}$  waves has been studied in much detail in mature ascidian eggs, by raising artificially the level of inositol 1,4,5-trisphosphate [ $\text{Ins}(1,4,5)\text{P}_3$ ] or of its poorly metabolizable analogue, glyceromyo-phosphatidylinositol 4,5-bisphosphate [ $\text{gPtdIns}(4,5)\text{P}_2$ ]. Here, we use this strategy and the experimental results it provides to develop a realistic theoretical model for repetitive  $\text{Ca}^{2+}$  wave generation and propagation in mature eggs. The model takes into account the heterogeneous spatial distribution of the endoplasmic reticulum. Our results corroborate the hypothesis that  $\text{Ca}^{2+}$  wave pacemakers are associated with cortical accumulations of endoplasmic reticulum. The model is first tested and validated by the adequate match between its theoretical predictions and the observed effects of localized injections of massive amounts of  $\text{Ins}(1,4,5)\text{P}_3$

analogues. In a second step, we use the model to make some propositions about the possible characteristics of the sperm factor. We find that to account for the spatial characteristics of the first series of  $\text{Ca}^{2+}$  waves seen at fertilization in ascidian eggs, it has to be assumed that, if the sperm factor is a phospholipase C, it is  $\text{Ca}^{2+}$ -sensitive and highly diffusible. Although the actual state of knowledge does not allow us to explain the observed relocation of the  $\text{Ca}^{2+}$  wave pacemaker site, the model corroborates the assumption that  $\text{PtdIns}(4,5)\text{P}_2$ , the substrate for phospholipase C is distributed over the entire egg. We also predict that the dose of sperm factor injected into the egg should modulate the temporal characteristics of the first, long-lasting fertilization wave.

Key words: Calcium waves, Fertilization, Ascidian, Sperm factor

## Introduction

In all eggs, fertilization induces a dramatic increase in cytosolic  $\text{Ca}^{2+}$ . This rise in  $\text{Ca}^{2+}$  occurs as a wave propagating through the whole egg from the site of sperm-egg fusion and drives egg activation (Stricker, 1999). In many species, including ascidians and mammals, this fertilization wave is followed by repetitive  $\text{Ca}^{2+}$  waves of shorter duration and smaller amplitude (McDougall and Sardet, 1995; Stricker, 1999) similar to those observed in a variety of somatic cells stimulated by hormones, growth factors or neurotransmitters (Berridge et al., 2000). Ascidian eggs moreover have the unique property of displaying two stereotypic series of  $\text{Ca}^{2+}$  waves (McDougall and Sardet 1995; Dumollard et al., 2002). Series I  $\text{Ca}^{2+}$  waves consist of the large amplitude fertilization wave, followed by a few smaller spikes. Series I lasts for about 8 minutes and drives meiosis I up to the extrusion of the first polar body.  $\text{Ca}^{2+}$  oscillations then stop for about 5 minutes. A second series of  $\text{Ca}^{2+}$  waves then resumes with a progressively increasing, and then decreasing amplitude. This series II lasts for 15-20 minutes, drives meiosis II and stops just before the extrusion of the second polar body (McDougall and Sardet, 1995).

It is known that in most cell types the signal-induced  $\text{Ca}^{2+}$  increases rely on the production of inositol 1,4,5-trisphosphate

[ $\text{Ins}(1,4,5)\text{P}_3$ ], a diffusible second messenger that activates  $\text{Ca}^{2+}$  release from the endoplasmic reticulum (ER). As the activity of the  $\text{Ins}(1,4,5)\text{P}_3$  receptor [ $\text{Ins}(1,4,5)\text{P}_3\text{R}$ ] is also stimulated by cytosolic  $\text{Ca}^{2+}$ , an initially localized  $\text{Ca}^{2+}$  increase triggers the regenerative propagation of the  $\text{Ca}^{2+}$  wave throughout the egg while sustained activation of the  $\text{Ins}(1,4,5)\text{P}_3\text{Rs}$  gives rise to  $\text{Ca}^{2+}$  oscillations and waves (Berridge et al., 2000).

A universal trigger for the initial  $\text{Ca}^{2+}$  release at fertilization has not yet been identified. Sperm-egg fusion can however be replaced by the injection of a soluble sperm extract (Swann and Parrington 1999; Runft et al., 2002). In mammals, it has been proposed that the active component of this sperm extract, known as sperm factor (SF), is a new isoform of phospholipase C (PLC) (the enzyme responsible for  $\text{Ins}(1,4,5)\text{P}_3$  synthesis) known as  $\text{PLC}\zeta$  (Saunders et al., 2002; Cox et al., 2002) (reviewed by Kurokawa et al., 2004). In ascidians, the key factor is an unidentified protein with a size of between 30 and 100 kDa (Kyoizuka et al., 1998). It could be either a soluble PLC or an unknown activator of PLC (Runft and Jaffe, 2000; Runft et al., 2002).

Given the pivotal role played by the  $\text{Ca}^{2+}$  dynamics in the activation of the egg and its development into an embryo

(Dupont, 1998; Ozil, 1998), a detailed understanding of the biochemical events responsible for the temporal and spatial organization of cytoplasmic  $\text{Ca}^{2+}$  signals at fertilization is required. To this aim, simulations provide a useful complementary approach to the numerous experimental studies.

The basic mechanism of  $\text{Ca}^{2+}$  oscillations in eggs does not differ much from that of  $\text{Ca}^{2+}$  oscillations in somatic cells. Most models ascribe the oscillations to the autocatalytic regulation exerted by cytoplasmic  $\text{Ca}^{2+}$  on its own release from the ER (Goldbeter et al., 1990; Sneyd et al., 1995) (Fig. 1). Some studies, however, stress the possible role of the activation of PLC by  $\text{Ca}^{2+}$ , a regulation that also leads to a regenerative increase in cytosolic  $\text{Ca}^{2+}$  (Meyer and Stryer, 1988; Hirose et al., 1999). Despite numerous theoretical approaches (reviewed by Schuster et al., 2002), no model until now has focussed on the rather typical shape of the repetitive  $\text{Ca}^{2+}$  waves that are triggered at fertilization.

Theoretically,  $\text{Ca}^{2+}$  wave propagation can be ascribed to the same regulatory processes as oscillations (Sneyd et al., 1995; Goldbeter, 1996). It is clear, however, that the detailed characteristics of the waves much depend on the cell type. In eggs, these waves can take the form of sharp fronts, spirals or tides (Lechleiter et al., 1991; McDougall and Sardet, 1995; Fontanilla and Nuccitelli, 1998). The detailed shape of the front can also vary: both convex and concave fronts have been observed (Stricker, 1999). Moreover, the large size of the eggs allows a clearer manifestation of the effects related with the spatial inhomogeneity of the cytoplasm. Distinct subcellular regions that repetitively initiate  $\text{Ca}^{2+}$  waves have been identified in the ascidian egg (McDougall and Sardet, 1995; Dumollard and Sardet, 2001; Dumollard et al., 2002). Three such regions, called 'calcium wave pacemakers (PM)', have been reported. (1) PM1 is defined as the initiation sites of the first series of  $\text{Ca}^{2+}$  oscillations (series I). PM1 is a moving  $\text{Ca}^{2+}$  wave pacemaker: the fertilization wave indeed initiates at the site of sperm entry, while the initiation sites of the subsequent waves progressively migrate with the sperm aster towards the vegetal contraction pole. (2) Pacemaker PM2 is stably localized in the vegetal contraction pole, a cortical constriction of 15–20  $\mu\text{m}$  in diameter. It is a region of dense ER and mitochondria accumulation. (3) An artificial pacemaker called PM3 is located in the animal hemisphere, and is defined as the cellular region most sensitive to an artificial stimulation by  $\text{Ins}(1,4,5)P_3$ . It probably corresponds to a region rich in ER clusters, present around the meiotic spindle in the mature unfertilized egg (Dumollard and Sardet, 2001).

Some theoretical models have already investigated the spatial characteristics of the  $\text{Ca}^{2+}$  increase occurring at fertilization (Wagner et al., 1998; Bugrim et al., 2003; Hunding and Ipsen, 2003). It was shown that the correct shape of the fertilization wave in *Xenopus* oocyte can be reproduced by assuming that  $\text{Ins}(1,4,5)P_3$  is locally generated at the fertilization site (Bugrim et al., 2003). Moreover, these studies emphasize the role of the spatial inhomogeneities in the ER distribution (Bugrim et al., 2003; Hunding and Ipsen, 2003), in the  $\text{Ins}(1,4,5)P_3$ R distribution (Bugrim et al., 2003) or in  $\text{Ins}(1,4,5)P_3$  production (Wagner et al., 1998) to reproduce the experimentally observed spatial profiles. None of these studies, however, deals with repetitive  $\text{Ca}^{2+}$  waves, as those observed at fertilization of many species, including ascidians and mammals. In the case of the *Xenopus* oocytes, the fertilization

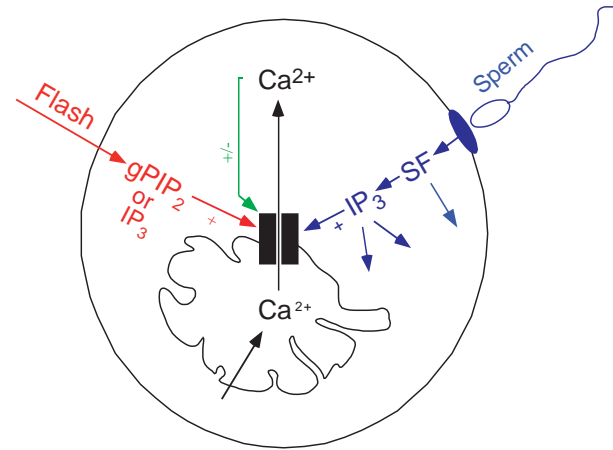


**Fig. 1.** Model developed to account for  $\text{Ca}^{2+}$  oscillations and waves in ascidian eggs. The red pathway shows experiments of  $\text{gPtdIns}(4,5)P_2$  ( $\text{gPIP}_2$ ) or  $\text{Ins}(1,4,5)P_3$  ( $\text{IP}_3$ ) flash photolysis, while the blue pathway shows the events supposed to occur at fertilization. The model is adapted from previous reports (Dupont and Swillens, 1996; Dupont and Erneux, 1997).

$\text{Ca}^{2+}$  wave is indeed seen as a switch in a bistable system. Recovery, i.e. return to the basal  $\text{Ca}^{2+}$  level, is seen to occur on a much longer time scale than the increase in  $\text{Ca}^{2+}$ .

In the present study, we simulate repetitive  $\text{Ca}^{2+}$  waves with a spatio-temporal pattern analogous to that of series I oscillations in ascidian eggs. We focus on the  $\text{Ca}^{2+}$  waves induced by  $\text{Ins}(1,4,5)P_3$  or its poorly metabolizable analogue glycerol-myoinositol 4,5-bisphosphate [ $\text{gPtdIns}(4,5)P_2$ ] and on series I  $\text{Ca}^{2+}$  oscillations. We first simulate an existing model for  $\text{Ca}^{2+}$  and  $\text{Ins}(1,4,5)P_3$  dynamics and show that it can reproduce the experimentally observed  $\text{Ca}^{2+}$  waves triggered by flash photolysis of  $\text{Ins}(1,4,5)P_3$  or  $\text{gPtdIns}(4,5)P_2$  when considering an appropriate inhomogeneous distribution of ER. We then show the results of simulations of the model predicting the effect of a localized injection of a large amount of  $\text{gPtdIns}(4,5)P_2$ . This prediction is confirmed experimentally. In a second part, we use our model to simulate the fertilization wave and the series I  $\text{Ca}^{2+}$  oscillations. We find that the best agreement with the experimental data is obtained if it is assumed that the SF in ascidian eggs is a  $\text{Ca}^{2+}$ -sensitive, highly diffusible PLC, and that  $\text{PtdIns}(4,5)P_2$ , the substrate for PLC, is homogeneously distributed in the whole egg.

## Model

### Evolution equations

In ascidian eggs,  $\text{Ca}^{2+}$  oscillations can be generated by a single and long-lasting increase of the poorly metabolizable analogue of  $\text{Ins}(1,4,5)P_3$ ,  $\text{gPtdIns}(4,5)P_2$  (Dumollard and Sardet, 2001) (see below); in such conditions,  $\text{Ca}^{2+}$  oscillations can be ascribed to the well-known biphasic regulation of the type I  $\text{Ins}(1,4,5)P_3$ R by  $\text{Ca}^{2+}$  (Bezprozvanny et al., 1991; Finch et al., 1991; Miyakawa et al., 1999). Moreover, only the type I  $\text{Ins}(1,4,5)P_3$ R can be found in the ascidian genome (<http://genome.jgi-psf.org/cgi-bin/searchGM2.cgi?db=ciona4>). The model used in the present study to describe the evolution

of the levels of  $\text{Ca}^{2+}$ ,  $\text{Ins}(1,4,5)\text{P}_3$  and active receptors is a modified version of a prototypic model describing the sequential activation-inhibition of the receptor as the level of cytosolic  $\text{Ca}^{2+}$  increases (Fig. 1) (Dupont and Swillens, 1996). The evolution of the fraction of receptor in an inactive (desensitized) state,  $R_{\text{des}}$ , is given by:

$$\frac{dR_{\text{des}}}{dt} = k_+(1 - R_{\text{des}}) \frac{C_{\text{cyto}}^{\text{ni}}}{1 + \left(\frac{C_{\text{cyto}}}{K_{\text{act}}}\right)^{n_a}} - k_- R_{\text{des}}, \quad (1)$$

where  $k_+$  is the rate of inhibition of the  $\text{Ins}(1,4,5)\text{P}_3\text{R}$  by cytosolic  $\text{Ca}^{2+}$  and  $k_-$  the rate of relief from this inhibition. Activation of the receptor by  $\text{Ca}^{2+}$  is assumed to be instantaneous and characterized by a threshold constant  $K_{\text{act}}$ . The level of cytosolic  $\text{Ca}^{2+}$  ( $C_{\text{cyto}}$ ) varies through  $\text{Ca}^{2+}$  release via the  $\text{Ins}(1,4,5)\text{P}_3\text{Rs}$  and  $\text{Ca}^{2+}$  pumping by  $\text{Ca}^{2+}$  ATPases located in the membrane of the ER. We do not consider  $\text{Ca}^{2+}$  exchanges with the extracellular medium, as it is known that  $\text{Ca}^{2+}$  oscillations in ascidian eggs can occur in the absence of extracellular  $\text{Ca}^{2+}$  (Speknsijder et al., 1989; Carroll et al., 2003). Taking diffusion into account, the evolution equation for the concentration of cytosolic  $\text{Ca}^{2+}$  can be written:

$$\frac{\partial C_{\text{cyto}}}{\partial t} = \lambda(r) \left[ \alpha(r) k_1 (b + \text{IR}_a) (C_{\text{lum}} - C_{\text{cyto}}) - V_{\text{MP}} \frac{C_{\text{cyto}}}{K_{\text{p}}^2 + C_{\text{cyto}}^2} \right] + D_{\text{cyto}} \frac{\partial^2 C_{\text{cyto}}}{\partial r^2}. \quad (2)$$

In this equation,  $\text{IR}_a$  represents the fraction of  $\text{Ins}(1,4,5)\text{P}_3\text{Rs}$  in an active state, and is given by:

$$\text{IR}_a = \frac{\text{IR}_{\text{able}}}{1 + \left(\frac{K_{\text{act}}}{C_{\text{cyto}}}\right)^{n_a}},$$

where

$$\text{IR}_{\text{able}} = (1 - R_{\text{des}}) \left[ \frac{\text{IP}}{K \left(1 + \frac{g\text{PtdIns}(4,5)\text{P}_2}{K_{\text{gPtdIns}(4,5)\text{P}_2}}\right) + \text{IP}} + \frac{g\text{PtdIns}(4,5)\text{P}_2}{K_{\text{gPtdIns}(4,5)\text{P}_2} \left(1 + \frac{\text{IP}}{K}\right) + g\text{PtdIns}(4,5)\text{P}_2} \right], \quad (3)$$

where  $\text{IP}$  and  $g\text{PtdIns}(4,5)\text{P}_2$  represent the  $\text{Ins}(1,4,5)\text{P}_3$  and the  $g\text{PtdIns}(4,5)\text{P}_2$  concentrations, respectively.  $g\text{PtdIns}(4,5)\text{P}_2$  is explicitly considered in the model, because we simulate experiments of flash-photolysis of this poorly metabolizable analogue of  $\text{Ins}(1,4,5)\text{P}_3$ . Parameter  $k_1$  fixes the rate of  $\text{Ca}^{2+}$  release through the  $\text{Ins}(1,4,5)\text{P}_3\text{R}$  and  $k_1 b$  is a leak term;  $C_{\text{lum}}$  stands for the concentration of free  $\text{Ca}^{2+}$  in the ER. The second term of equation (2) represents the pumping of  $\text{Ca}^{2+}$  into the

ER by the ATPases. The last term is a classical Fick term for diffusion.

The distribution of ER is taken into account through two parameters:  $\lambda$  and  $\alpha$ , which are both functions of space ( $r$ ) to allow heterogeneity. Two parameters are necessary because the amount of ER affects both the number of  $\text{Ins}(1,4,5)\text{P}_3\text{Rs}$  and  $\text{Ca}^{2+}$  pumps (located in the ER membrane), and the local volumes of the ER and cytosol, respectively. Thus, the first parameter ( $\lambda$ ) scales the number of channels [ $\text{Ins}(1,4,5)\text{P}_3\text{Rs}$  and  $\text{Ca}^{2+}$  pumps] and similarly affects all flux terms across the ER membrane. The other parameter ( $\alpha$ ) is defined as the local ratio between the volumes of the endoplasmic reticulum and the cytosol. It accounts for example for the fact that the release of a given number of moles of  $\text{Ca}^{2+}$  from the ER will induce a lower increase of the  $\text{Ca}^{2+}$  concentration in the cytosol than the associated decrease of  $\text{Ca}^{2+}$  concentration in the ER, due to the different volumes of these compartments. In this study, we always assume that the distribution of ER follows the same distribution than that of  $\text{Ca}^{2+}$  channels (Fink et al., 2000). Thus, there is a fixed relationship between  $\lambda(r)$  and  $\alpha(r)$ : assuming a spherical shape for the ER, any change in ' $\alpha$ ' of a factor ' $x$ ' will be accompanied by a change in  $\lambda$  of a factor  $x^{2/3}$ , given the surface/volume ratio of a sphere. In the following, we will discuss changes in ER distribution in terms of  $\alpha$ .

In contrast to other models, we do not assume that the  $\text{Ca}^{2+}$  concentration inside the ER remains constant, as the fertilization  $\text{Ca}^{2+}$  wave implies a massive release of  $\text{Ca}^{2+}$  from the ER. In our model, the evolution of the concentration of  $\text{Ca}^{2+}$  inside the ER lumen ( $C_{\text{lum}}$ ) is given by:

$$\frac{\partial C_{\text{lum}}}{\partial t} = \lambda(r) \left[ \frac{V_{\text{MP}}}{\alpha(r)} \frac{C_{\text{cyto}}}{K_{\text{p}}^2 + C_{\text{cyto}}^2} - k_1 (b + \text{IR}_a) (C_{\text{lum}} - C_{\text{cyto}}) \right] + D_{\text{ER}} \frac{\partial^2 C_{\text{lum}}}{\partial r^2}. \quad (4)$$

Implicit in the latter equation is the fact that the ER behaves as a continuous compartment invading the whole egg. In Equations (2) and (4), all fluxes must be seen as effective ones, as  $\text{Ca}^{2+}$  buffers are not explicitly incorporated in the model.

Finally,  $\text{Ins}(1,4,5)\text{P}_3$  is assumed to be synthesized from  $\text{PtdIns}(4,5)\text{P}_2$  by PLC and degraded by both a phosphatase and a kinase. Thus, the evolution of the concentration of  $\text{Ins}(1,4,5)\text{P}_3$  (IP) follows:

$$\frac{\partial \text{IP}}{\partial t} = I_{\text{IP}} + V_{\text{PLC}} - V_{5\text{P}} \frac{\text{IP}}{K_{5\text{P}} + \text{IP}} - V_{3\text{K}} \frac{\text{IP}}{K_{3\text{K}} + \text{IP}} \frac{C_{\text{cyto}}}{K_{\text{A}3\text{K}} + C_{\text{cyto}}} + D_{\text{IP}} \frac{\partial^2 \text{IP}}{\partial r^2}. \quad (5)$$

$I_{\text{IP}}$  [for  $\text{Ins}(1,4,5)\text{P}_3$  input] allows us to simulate the experiments of  $\text{Ins}(1,4,5)\text{P}_3$  flash-photolysis (in this case, this parameter takes a non-zero value during the simulated flash).  $V_{\text{PLC}}$  represents the basal rate of  $\text{Ins}(1,4,5)\text{P}_3$  synthesis in a non-fertilized egg. In equation (5), this rate is assumed to be  $\text{Ca}^{2+}$ -insensitive, in the absence of further indication as to the PLC isoform present in the ascidian egg. However, given that  $V_{\text{PLC}}$  is a small term [because it must lead to a basal low level of  $\text{Ins}(1,4,5)\text{P}_3$ ] the behaviour of the model remains

unchanged if  $V_{PLC}$  is made  $Ca^{2+}$ -sensitive.  $V_{5P}$  and  $V_{3K}$  stand for the maximal rates of  $Ins(1,4,5)P_3$ -5-phosphatase and -3-kinase, respectively, while  $K_{5P}$  and  $K_{3K}$  are the Michaelis constants of the same enzymes. Stimulation of  $Ins(1,4,5)P_3$ -3-kinase activity by  $Ca^{2+}$  is taken into account; the constant for half-maximal activation is represented by  $K_{A3K}$ . As discussed below, the concentration of  $PtdIns(4,5)P_2$  (the substrate for PLC) is assumed to be homogeneous throughout the whole egg and to remain constant or at least not limiting (Xu et al., 2003).

### Inhomogeneities in the endoplasmic reticulum distribution

The ascidian egg is a large cell, the diameter of which is comprised between 100 and 150  $\mu m$ . As many other eggs, the cytoplasm is highly structured in specific domains that host different concentrations of intracellular organelles (mitochondria, yolk platelets and endoplasmic reticulum). It is also known that a spectacular reorganization of these egg structures occurs at fertilization (Roegiers et al., 1999). In particular, a wave of cortical contraction leads to the formation of the contraction pole in the vegetal hemisphere, a region containing an accumulation of cortical ER (Roegiers et al., 1999; Dumollard and Sardet, 2001). As we focus here on the  $Ca^{2+}$  changes induced by the injection of  $Ins(1,4,5)P_3$  or  $Ins(1,4,5)P_3$  analogues, or occurring just after fertilization, we do not consider these rearrangements in the present study. As a first hypothesis, we only consider inhomogeneities in the ER distribution (parameters  $\alpha$  and  $\lambda$ ) to test if those are sufficient to account for the observed  $Ca^{2+}$  wave initiation sites. To simplify the simulations, we have chosen a 2D geometry. This assumption amounts to looking at a slice through the egg, but introduces a bias on the value of the fluxes. However, as most parameter values are not known for the ascidian eggs, we think that this assumption (which much reduces the computing time) is worthwhile.

The ER is modelled as a continuous network of varying density throughout the cytosol. Thus parameter  $\alpha$ , defined as the ratio between the volumes occupied by the endoplasmic reticulum and by the cytosol, is a function of space ( $r$ ). As suggested by direct observations on mature eggs (Dumollard and Sardet., 2001; Sardet et al., 2002), we assume that the density of the reticulum is higher in the cortex than in the cytosol. The thickness of this higher density region is of a few microns. In the model, it is assumed that there is a gradient of reticular density from the periphery to the centre, given by:

$$\alpha'(r) = \alpha_B \left( 1 + \alpha_C e^{\frac{r-r_c}{w}} \right), \quad (6)$$

where  $\alpha_B$  is the basal density of ER,  $\alpha_C$  reflects the amplitude of the gradient,  $r_c$  is the radius of the egg and  $w$  reflects the steepness of the gradient. The spatial coordinate  $r$  is calculated in a system centred on the centre of the egg.

Moreover, we consider another type of inhomogeneity strongly suggested by recent experimental observations; it has been shown that the artificial pacemaker located in a broad cortical region of the animal hemisphere (PM3) serves as the initiation site of the  $Ca^{2+}$  waves induced by exogenous

injections of  $Ins(1,4,5)P_3$  or  $gPtdIns(4,5)P_2$  (Dumollard and Sardet, 2001). We thus use numerical simulations to investigate the hypothesis that a higher density of ER suffices to explain all the observations performed with respect to this new pacemaker. To account for the possible existence of such a region, we assume that  $\alpha$  is maximal at the cortex of the animal pole and linearly decreases towards the centre of the egg (vertical variation only). Thus, in the region called pacemaker 3 (PM3),

$$\alpha(r) = \alpha'(r) - \frac{h}{d} y + h \quad \text{if } y \leq d, \quad (7)$$

where  $y$  stands for the vertical distance from the upper point of the egg,  $h$  for the maximal increment of ER density and  $d$  for the characteristic length of the pacemaker region. The ER distribution defined by equations (6) and (7) is assumed to remain unchanged in the course of the simulations.

The resulting distribution of the ER for our particular set of parameter values is shown in Fig. 2. The average density of the ER is 8%, which is of the order of experimental measurements performed in other cell types (Depierre and Dallner, 1975; Fink et al., 2000). The resting cytosolic and luminal  $[Ca^{2+}]$  result from an equilibrium between  $Ca^{2+}$  fluxes across the ER membranes; in consequence, the steady-state level of  $Ca^{2+}$  in the absence of stimulation depends on ER density and this level of  $Ca^{2+}$  is inhomogeneous both in the cytosol and in the lumen. Although in the ER this inhomogeneity is not significant, cytosolic  $Ca^{2+}$  varies from 0.106  $\mu M$  to 0.167  $\mu M$  depending on the ER density (the higher the density, the higher the concentration). This effect is due to the locally lower cytosolic

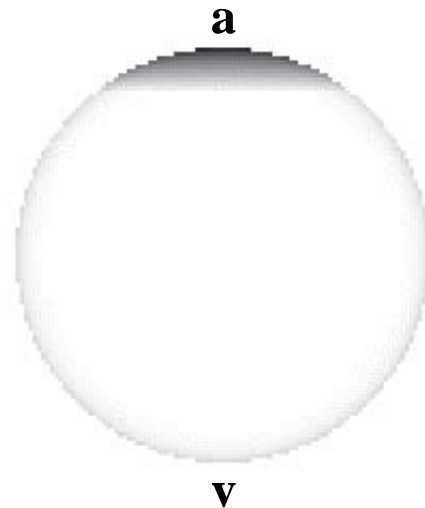


**Fig. 2.** Grey-scale representation of the density of the endoplasmic reticulum (parameter  $\alpha$ ) used in the simulations of  $Ca^{2+}$  oscillations and waves in ascidian eggs. The ER is assumed to be more concentrated in the cortex of the egg, with a maximal value in the animal cortex. Parameter  $\alpha$  measures the local ratio between the ER and the cytosolic volumes. Scale: black,  $\alpha=0.12$ ; white,  $\alpha=0.07$ . This ER density is given by equations (6) and (7) with the following parameter values to characterize the gradient of ER-density from the periphery to the center and the shape of the pacemaker (see text): basal density of ER  $\alpha_B=0.07$ ,  $\alpha_C=0.10$ ,  $w=0.04$ ,  $r_c=75 \mu m$ ,  $h=0.04$  and  $d=15 \mu m$ . a, animal pole; v, vegetal pole.

volume in the regions of high ER density (parameter  $\alpha$ ). By contrast, variations in  $\lambda$  affect both release and pumping and do thus not affect the steady-state levels of  $\text{Ca}^{2+}$ .

### Sperm factor

In the last part of our study, we investigate the sperm factor hypothesis. We start from the basic assumption that SF is a soluble PLC (Swann, 1996; Saunders et al., 2002; Cox et al., 2002; Howell et al., 2003). Thus, we simulate fertilization by assuming that a large amount of PLC is locally introduced in the egg. This additional PLC is superimposed on the basal PLC activity of the egg. SF is assumed to diffuse and to be degraded. The value of the diffusion coefficient will be discussed later. The time scale of SF degradation is chosen to fit the observed duration of series I  $\text{Ca}^{2+}$  oscillations in ascidian eggs. We also made the assumption that the activity of the injected PLC is stimulated by cytosolic  $\text{Ca}^{2+}$  (see below for the justification of this hypothesis). Thus, when modelling fertilization, a new equation describing the evolution of the level of sperm factor activity is introduced:

$$\frac{\partial \text{SF}}{\partial t} = -k_{\text{SF}}\text{SF} + D_{\text{SF}} \frac{\partial^2 \text{SF}}{\partial r^2}, \quad (8)$$

where  $k_{\text{SF}}$  stands for the rate constant of SF degradation and  $D_{\text{SF}}$  for the diffusion coefficient. Introduction of SF occurs through appropriate initial conditions. Moreover, equation (5) is modified to take into account the PLC activity of the SF:

$$\frac{\partial \text{IP}}{\partial t} = V_{\text{PLC}} + V_{\text{SF}}[\text{SF}] \frac{C_{\text{cyto}}}{K_{\text{ASF}}^2 + C_{\text{cyto}}} - V_{5\text{P}} \frac{\text{IP}}{K_{5\text{P}} + \text{IP}} - V_{3\text{K}} \frac{\text{IP}}{K_{3\text{K}} + \text{IP}} \frac{C_{\text{cyto}}}{K_{\text{A3K}} + C_{\text{cyto}}} + D_{\text{IP}} \frac{\partial^2 \text{IP}}{\partial r^2}. \quad (5')$$

$K_{\text{ASF}}$  is the threshold constant characterizing the stimulation of the PLC activity of the SF by  $\text{Ca}^{2+}$ . The values of  $V_{\text{PLC}}$  and  $V_{\text{SF}}$  are taken as constant in the whole egg, based on the assumption that  $\text{PtdIns}(4,5)\text{P}_2$  is homogeneously distributed (see 'Simulation of the series I  $\text{Ca}^{2+}$  oscillations induced by fertilization').

### Simulation method

Numerical simulations have been performed using a variable time-step Gear method. To simulate diffusion, the Laplacian is made discrete using the finite difference method. The egg is divided into mesh points, using a cartesian grid with no flux boundary conditions. The circular shape of the egg is reproduced by applying the appropriate no-flux boundary conditions at all grid points located at a given distance from the centre (corresponding to the egg radius). The egg radius is 75  $\mu\text{m}$  and the mesh size is 1.5  $\mu\text{m}$ .

## Results

An artificial pacemaker site (PM3) is revealed by flash-photolysis of  $\text{Ins}(1,4,5)\text{P}_3$  or  $\text{gPtdIns}(4,5)\text{P}_2$

Experimentally, caged  $\text{Ins}(1,4,5)\text{P}_3$  was photo-released either locally (i.e. the flash was restricted to a small region of the egg)

or globally (Dumollard and Sardet, 2001). The amount of  $\text{Ins}(1,4,5)\text{P}_3$  released is set by the duration of the UV flash and always remains rather small (less than 0.1  $\mu\text{M}$ ). Flash-photolysis of increasing amounts of  $\text{Ins}(1,4,5)\text{P}_3$  initiated a  $\text{Ca}^{2+}$  wave that spreads further from the site of the UV-flash. This observation is reproduced by the model (Fig. 3). The  $\text{Ca}^{2+}$  wave remains limited to a portion of the egg for  $\text{Ins}(1,4,5)\text{P}_3$  flashes of short duration because, in these cases, passive diffusion of  $\text{Ins}(1,4,5)\text{P}_3$  remains localized. Only when the amount of released  $\text{Ins}(1,4,5)\text{P}_3$  is large enough (Fig. 3, third row) does the level of  $\text{Ins}(1,4,5)\text{P}_3$  reach the threshold required to trigger a  $\text{Ca}^{2+}$  wave that traverses the whole egg.  $\text{Ins}(1,4,5)\text{P}_3$  can thus induce spatially restricted  $\text{Ca}^{2+}$  signals and  $\text{Ins}(1,4,5)\text{P}_3$  does not act as a global messenger in a large cell, such as the ascidian egg. For the parameter values used in the simulations, the characteristic time for  $\text{Ins}(1,4,5)\text{P}_3$  diffusion (80 seconds) is larger than that of  $\text{Ins}(1,4,5)\text{P}_3$  degradation (about 12 seconds).

Also in agreement with a relatively fast degradation of  $\text{Ins}(1,4,5)\text{P}_3$ , activation of the eggs by a single injection of  $\text{Ins}(1,4,5)\text{P}_3$  cannot induce repetitive  $\text{Ca}^{2+}$  waves, neither in the model, nor in the experiments. As modelled above (Fig. 3) and observed in the experiments (Dumollard and Sardet, 2001), when the  $\text{Ins}(1,4,5)\text{P}_3$  flashes are localized, the  $\text{Ca}^{2+}$  wave originates from the site of  $\text{Ins}(1,4,5)\text{P}_3$  release. More surprisingly, when  $\text{Ins}(1,4,5)\text{P}_3$  or its poorly metabolizable analogue  $\text{gPtdIns}(4,5)\text{P}_2$ , is homogeneously increased in the whole egg, the  $\text{Ca}^{2+}$  wave is always seen to originate from the cortex, in a broad area near the animal pole of the eggs (Dumollard and Sardet, 2001). As proposed in the experimental study, the existence of this pacemaker revealed by an artificial type of stimulation (called PM3) can be ascribed to a denser distribution of ER near the cortex of the animal pole. We have tested this hypothesis in the model. In Fig. 4,  $\text{gPtdIns}(4,5)\text{P}_2$  is assumed to be homogeneously released in the whole egg. However, the  $\text{Ca}^{2+}$  wave clearly initiates in the region with the highest density of ER (see Fig. 2 for the distribution of the ER). The shape of this region of higher density (see 'Inhomogeneities in the endoplasmic reticulum distribution') has been fitted in the simulations to get the best agreement with the experimentally observed forms of the  $\text{Ca}^{2+}$  wave. The best results are thus obtained when the gradient in  $\alpha$  (ER density) is only vertical (along the animal-vegetal axis). Equally important for the appropriate shape of the  $\text{Ca}^{2+}$  wave is the slightly more elevated quantity of ER in the cortex. Because of this inhomogeneity, the wave propagates faster in the periphery, allowing for the transformation of a convex front at the onset of the propagation into a slightly concave one as the wave spreads through the egg (Fig. 4), as seen in the experiments.

From a theoretical point of view,  $\alpha$  (ER density) is a bifurcation parameter. In other words, increasing the value of  $\alpha$  qualitatively changes the behaviour of the system, from resting, to excitable and finally to oscillatory. Thus, at a given fixed level of stimulation [ $\text{Ins}(1,4,5)\text{P}_3$  or  $\text{gPtdIns}(4,5)\text{P}_2$ ], the cytoplasm is excitable for eliciting a  $\text{Ca}^{2+}$  wave only when  $\alpha$  is above a critical level. The values of  $\alpha$  and of the stimulation intensity used in Fig. 4 are such that PM3 is the only part of the egg initially able to generate a  $\text{Ca}^{2+}$  spike. In the rest of the cytoplasm and in the cortex, the synergy between this low level of stimulus and the  $\text{Ca}^{2+}$  increase coming through diffusion from an adjacent region of the cell is required to generate a  $\text{Ca}^{2+}$  spike.

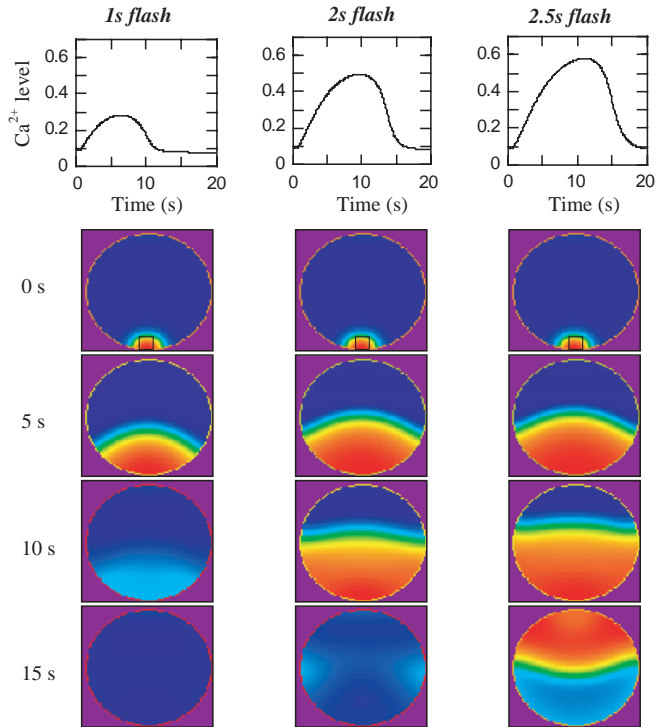


**Fig. 3.** Simulations of the effect of localized  $\text{Ins}(1,4,5)\text{P}_3$  injections. Results have been obtained by integration of equations (1) to (5) with the ER density represented in Fig. 2 and the following parameter values:  $D_{\text{cyto}}=40 \mu\text{m}^2 \text{second}^{-1}$ ,  $D_{\text{ER}}=4 \mu\text{m}^2 \text{second}^{-1}$ ,  $D_{\text{IP}}=280 \mu\text{m}^2 \text{second}^{-1}$ ,  $K_{\text{act}}=0.54 \mu\text{M}$ ,  $K_{\text{inh}}=(k_-/k_+)^{1/n_i}$   $0.28 \mu\text{M}$ ,  $k_-=4 \cdot 10^{-3} \text{second}^{-1}$ ,  $k_1=1.285 \text{second}^{-1}$ ,  $b=2.5 \cdot 10^{-4} \text{second}^{-1}$ ,  $K=1 \mu\text{M}$ ,  $v_{\text{MP}}=1.2 \mu\text{M second}^{-1}$ ,  $K_{\text{P}}=0.35 \mu\text{M}$ ,  $V_{\text{PLC}}=0.015 \mu\text{M second}^{-1}$ ,  $V_{5\text{P}}=0.67 \mu\text{M second}^{-1}$ ,  $K_{5\text{P}}=8 \mu\text{M}$ ,  $V_{3\text{K}}=3.35 \cdot 10^{-2} \mu\text{M second}^{-1}$ ,  $K_{3\text{K}}=0.5 \mu\text{M}$ ,  $K_{\text{A3K}}=0.3 \mu\text{M}$ ,  $n_a=2$ ,  $n_i=3$ . Most of these values come from previous modelling studies, where they were either taken from the literature or fitted to get agreement with the observations (Dupont and Erneux, 1997; Dupont et al., 2000). In the three simulations, during the flash time  $I_{\text{IP}}=7 \mu\text{M second}^{-1}$  in the mesh points (46 to 54) along the X axis, and (89 to 97) along the Y axis (this region is indicated as a black square in the first panel). The resulting  $\text{Ins}(1,4,5)\text{P}_3$  increase taken as an average on the whole egg ranges between 0.05 and 2.5  $\mu\text{M}$  depending on the flash duration. Initial conditions are  $C_{\text{cyto}}=0.1 \mu\text{M}$ ,  $C_{\text{lum}}=875 \mu\text{M}$  and the corresponding steady-state values of the other variables. To perform the simulations, mesh points are labelled 1 to 100 from left to right, and from top to bottom. To account for the circular shape of the egg (in two dimensions), the appropriate mesh points are excluded from the system. In this and all subsequent figures, the level of cytosolic  $\text{Ca}^{2+}$  is represented by the amount of  $\text{Ca}^{2+}$  bound to an indicator whose  $K_{1/2}$  for  $\text{Ca}^{2+}$  is  $0.7 \mu\text{M}$ . When representing the  $\text{Ca}^{2+}$  waves, the scale is different for each image, with red and blue representing the highest and the lowest instantaneous levels of cytosolic  $\text{Ca}^{2+}$ , respectively.

The level of stimulation [simulated here in the form of the amplitude of the  $\text{gPtdIns}(4,5)\text{P}_2$  influx] can also be viewed as a bifurcation parameter. The model accounts for the experimental observation (Dumollard and Sardet, 2001) that the global amplitude and the propagation velocity of the  $\text{Ca}^{2+}$  wave both increase with the amount of  $\text{gPtdIns}(4,5)\text{P}_2$  released into the egg (Fig. 5). These increases in  $\text{Ca}^{2+}$  wave amplitude are associated with a widening of the  $\text{Ca}^{2+}$  front but the local maximal amplitudes do not change when varying the level of

stimulation (not shown). The wave-like behaviour exemplified in Fig. 4 is restricted to a limited range of stimulation levels. In both the model and the experiments, if the magnitude of the global  $\text{gPtdIns}(4,5)\text{P}_2$  increase is too low (below  $0.03 \mu\text{M second}^{-1}$ ), it only generates a spatially limited  $\text{Ca}^{2+}$  increase confined to the animal pole region. By contrast, for the largest influx terms (above  $0.05 \mu\text{M second}^{-1}$ ), the  $\text{Ca}^{2+}$  increase occurs simultaneously in the entire egg. For all situations represented in Fig. 5, the local variations of ER  $\text{Ca}^{2+}$  associated with the wave of cytosolic  $\text{Ca}^{2+}$  are very small given the high level of  $\text{Ca}^{2+}$  in this compartment. We have taken an initial value of  $875 \mu\text{M}$  for the  $\text{Ca}^{2+}$  concentration in the ER (Montero et al., 1995; Hofer and Schulz, 1996).

In contrast to  $\text{Ins}(1,4,5)\text{P}_3$ ,  $\text{gPtdIns}(4,5)\text{P}_2$  is very slowly metabolized and its level remains elevated for a long time. As a consequence, several  $\text{Ca}^{2+}$  spikes can be generated by a single flash. The model can reproduce this behaviour if the rate of degradation of  $\text{gPtdIns}(4,5)\text{P}_2$  is assumed to be ten times smaller than that of  $\text{Ins}(1,4,5)\text{P}_3$  degradation as it was found experimentally (Bird et al., 1992). Fig. 6A indeed shows that in response to a localized  $\text{gPtdIns}(4,5)\text{P}_2$  increase of high amplitude, two  $\text{Ca}^{2+}$  waves are generated; the first one originates from the region of stimulation (here chosen to be in the vegetal pole), while the second one starts in the region of higher ER density in the animal pole region (PM3). A close look at the evolution of the variables of the model indicates that at that time (125 seconds),  $\text{gPtdIns}(4,5)\text{P}_2$  is homogeneously distributed in the egg; the second wave thus originates from the region that is the most sensitive to a homogeneous level of  $\text{gPtdIns}(4,5)\text{P}_2$ . This prediction is corroborated by the experimental results shown in Fig. 6B.

#### Injections of large amounts of $\text{gPtdIns}(4,5)\text{P}_2$ mimic the temporal pattern of $\text{Ca}^{2+}$ seen at fertilization

Large amounts of  $\text{gPtdIns}(4,5)\text{P}_2$  globally released in the egg induce a complex series of  $\text{Ca}^{2+}$  increases that strikingly resemble the first phase of  $\text{Ca}^{2+}$  waves observed at fertilization of ascidian eggs (Dumollard and Sardet, 2001). Fig. 7 shows the simulation of the injection of a large amount of  $\text{gPtdIns}(4,5)\text{P}_2$  (red trace). At time 0, the concentration of the latter compound is increased up to a high value; it then decreases to zero according to equation (5), in which the maximal velocities have been adapted for  $\text{gPtdIns}(4,5)\text{P}_2$  [instead of  $\text{Ins}(1,4,5)\text{P}_3$ ; see legend to Fig. 4]. The high level of  $\text{gPtdIns}(4,5)\text{P}_2$  causes a long-lasting  $\text{Ca}^{2+}$  increase, followed by two shorter spikes (black trace). Also visible are the changes of  $\text{Ca}^{2+}$  concentration within the ER (blue trace); note that  $\text{Ca}^{2+}$  depletion of the ER (up to  $\sim 40\%$ ) is significant only for the first  $\text{Ca}^{2+}$  increase. As far as the spatial aspects are concerned, the first massive  $\text{Ca}^{2+}$  increase propagates so rapidly that it seems to occur quasi-instantaneously in the whole egg. The second (and other subsequent) peaks clearly originate from the cortical area of the animal hemisphere, which possesses the highest ER density. These theoretical results are in full agreement with the experimental results (see Fig. 3B of Dumollard and Sardet, 2001).

#### Simulation of the series I $\text{Ca}^{2+}$ oscillations induced by fertilization

Given the observed agreement between our simulations and the experimental observations, we have used the model to make

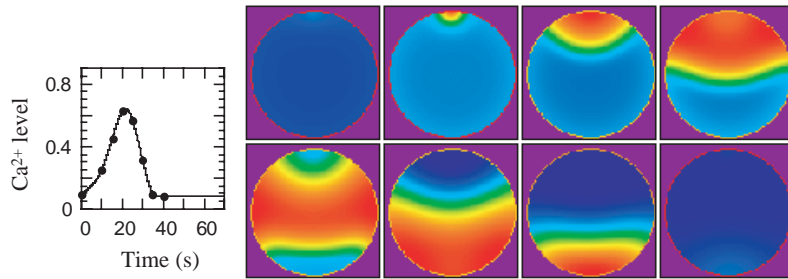


**Fig. 4.** Simulation of the effect of a global increase in  $[gPtdIns(4,5)P_2]$ . Results have been obtained by integration of equations (1) to (5) with the ER density represented in Fig. 2 and the same parameter values as in Fig. 3, except for the fact that  $gPtdIns(4,5)P_2$  has been used instead of  $Ins(1,4,5)P_3$ . Thus the rates of degradation ( $V_{5P}$  and  $V_{3K}$ ) have been divided by ten. To simulate the activation of the  $Ins(1,4,5)P_3R$  by both  $gPtdIns(4,5)P_2$  and the basal  $Ins(1,4,5)P_3$  level, we must replace the second part of equation (3) by:

$$IR_{\text{able}} = (1 - R_{\text{des}}) \left[ \frac{IP}{K \left( 1 + \frac{gPtdIns(4,5)P_2}{K_{gPtdIns(4,5)P_2}} \right) + IP} + \frac{gPtdIns(4,5)P_2}{K_{gPtdIns(4,5)P_2} \left( 1 + \frac{IP}{K} \right) + gPtdIns(4,5)P_2} \right],$$

with  $K_{gPtdIns(4,5)P_2} = 8 \mu\text{M}$ . These latter changes reflect the facts that  $gPtdIns(4,5)P_2$  is slowly metabolized and that  $Ins(1,4,5)P_3$  and  $gPtdIns(4,5)P_2$  bind to the same site of the receptor, and that  $gIns(4,5)P_2$  has less affinity for the receptor. A basal level of  $Ins(1,4,5)P_3$  equal to 18 nM (corresponding to the stationary state in  $Ins(1,4,5)P_3$  with the basal LC activity) is always present. During the flash time (2 seconds),  $I_{gPtdIns(4,5)P_2} = 0.045 \mu\text{M second}^{-1}$  in the whole system. The successive panels show the spatial distribution of  $Ca^{2+}$  at the times indicated by the points on the curve on the left.

some theoretical predictions about the possible nature of the sperm factor (SF). We simulate fertilization as a localized rise in SF concentration from zero up to an arbitrary value. If we assume that the SF is a  $Ca^{2+}$ -sensitive PLC that can diffuse in the cytosol [equations (5') and (8)], the model reproduces the temporal pattern of cytosolic  $Ca^{2+}$  changes observed at fertilization of ascidian eggs (Fig. 8). The level of PLC activity rises instantaneously (corresponding to the injection of SF) and then decays exponentially, due to the first-order degradation term. As for  $Ins(1,4,5)P_3$ , it massively rises with the step-wise increase in PLC; it then globally decays due to its catabolism by the  $Ins(1,4,5)P_3$  3-kinase and 5-phosphatase and to the decrease in PLC. However, because of the stimulation of PLC activity by  $Ca^{2+}$ , the concentration of  $Ins(1,4,5)P_3$  oscillates in synchrony with  $Ca^{2+}$  oscillations (Meyer and Stryer, 1988).

The spatial properties of the  $Ca^{2+}$  oscillations shown in Fig. 8 have not yet been investigated in the model. Simulations of the moving pacemaker observed in series I  $Ca^{2+}$  oscillations (PM1) of the ascidian egg indeed require both additional hypotheses and new simulation techniques. It may be that the source of  $Ins(1,4,5)P_3$  is moving along the cortex as a consequence of the cortical contraction-induced movement of the sperm aster towards the vegetal hemisphere (Dumollard and Sardet, 2001; Dumollard et al., 2002; Carroll et al., 2003).

We have assumed that the  $Ca^{2+}$ -sensitive PLC supposed to represent the SF has a relatively high diffusion coefficient ( $150 \mu\text{m}^2 \text{second}^{-1}$ ). If this is not the case, partial  $Ca^{2+}$  waves propagating only in the region of the egg opposite to the site of SF increase are observed, while the  $[Ca^{2+}]_c$  remains constantly elevated in the region closer to the injection site (not shown). This is owing to the fact that far away from the site of SF increase, the level of  $Ins(1,4,5)P_3$  is still in the oscillatory regime, because the level of PLC in this region is relatively low as significant diffusion has not yet occurred.

Finally, we have investigated in the model the effect of changing the amount of SF injected into the egg. As shown in Fig. 9, our preliminary model predicts that the amount of SF influences the shape of the first large fertilization spike. As expected intuitively, the duration of the fertilization spike increases with the dose of SF introduced into the egg. Interestingly, the shape of the spike also depends on the dose of SF. The number of small-amplitude spikes superimposed on the plateau increase of  $Ca^{2+}$  rises if the dose of SF decreases. For lower doses of SF (Fig. 9A), the level of  $Ins(1,4,5)P_3$  is close to that able to induce oscillations. By contrast, if  $[SF]$  is large (Fig. 9B), the  $Ins(1,4,5)P_3$  concentration is so high that  $Ca^{2+}$  remains at a high steady-state level set by the actual  $Ins(1,4,5)P_3$  concentration.

## Discussion

To our knowledge, we have presented here the first theoretical study devoted to the specific characteristics of the oscillatory  $Ca^{2+}$  signal occurring at fertilization. Our approach relies on the experimental observations performed previously (Dumollard and Sardet, 2001). The ability to model the experiments of flash photolysis of caged  $Ins(1,4,5)P_3$  and its analogue first allowed us to focus on the events downstream from  $Ins(1,4,5)P_3$  generation; we were able to 'fit' our equations and parameter values to describe adequately the  $Ca^{2+}$  dynamics

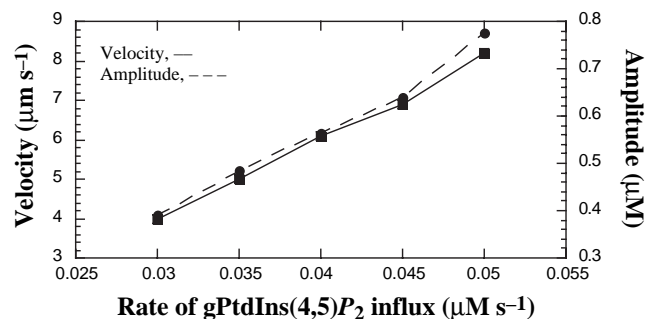
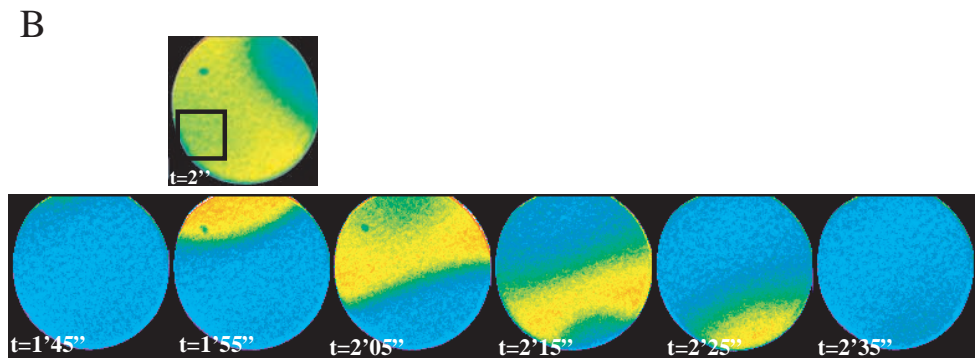
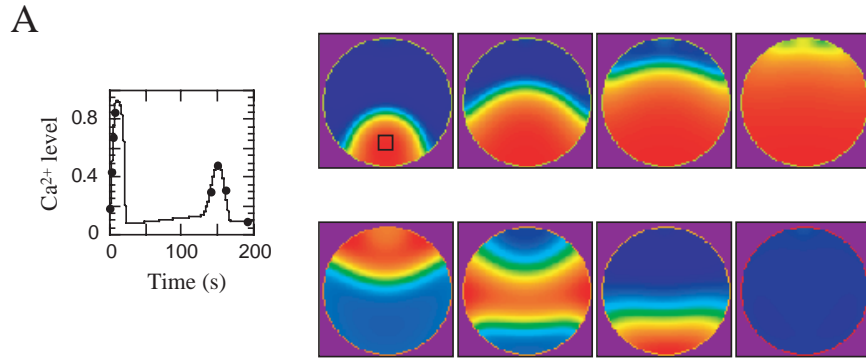


**Fig. 5.** Relationship between the mean velocity and global amplitude of the artificially induced  $Ca^{2+}$  waves and the intensity of the stimulus. Points have been obtained as in Fig. 4 with the same parameter values, except for the rate of  $gPtdIns(4,5)P_2$  influx. For influx rates lower than  $0.03 \mu\text{M second}^{-1}$ , the  $Ca^{2+}$  waves do not propagate throughout the whole egg (abortive waves). Conversely, for influx rates higher than  $0.05 \mu\text{M second}^{-1}$ , the  $Ca^{2+}$  increases occur nearly homogeneously over the whole egg.

**Fig. 6.** (A) Theoretical prediction of the effect of a gPtdIns(4,5) $P_2$  increase in the vegetal hemisphere of the ascidian egg. A high amplitude increase in gPtdIns(4,5) $P_2$  initiated in the vegetal hemisphere of the egg (indicated by a black square) evokes two successive  $Ca^{2+}$  waves, the first one emanating from the locus of stimulation and the second one emanating from the region of higher ER density in the animal pole region (PM3). Simulations have been performed as in Fig. 4 with a gPtdIns(4,5) $P_2$  increase

$I_{gPtdIns(4,5)P_2} = 12 \mu M \text{ second}^{-1}$  for 4 seconds, at the mesh points (45 to 55) along the X axis and (80 to 90) along the Y axis, as indicated by the black box in the first panel. The successive panels show the spatial distribution of  $Ca^{2+}$  at the times indicated by the points on the curve on the left.

(B) Effect of local photo-release of gPtdIns(4,5) $P_2$  in an unfertilized ascidian egg. First row: confocal image of  $[Ca^{2+}]_c$  (the concentration of cytosolic  $Ca^{2+}$ ) taken 2 seconds (2'') after local UV uncaging, the area of UV uncaging is indicated by a black square. Second row: a  $Ca^{2+}$  wave is initiated at 1 minute 45 seconds ( $t=1'45''$ ) in the animal pole and traverses the whole egg.



observed experimentally. Moreover, to account for the observed spatial characteristics of these artificial waves, we were led to make some reasonable assumptions about the ER distribution in the cortex and cytoplasm. For this first part of the study, we would like to stress the following results.

(1) If the ER density is modelled by taking into account the respective volumes accessible to both compartments (the ER and the cytosol), it represents a bifurcation parameter that can

determine the excitability of a given part of the cell, unlike in other existing models (Wagner et al., 1998; Fink et al., 2000; Bugrim et al., 2003; Hunding et al., 2003). Under these conditions, the regions with higher ER density naturally play the role of pacemaker sites. This assumption also allowed us to make an experimental prediction about the initiation site of the successive waves induced by the local release of high doses of gPtdIns(4,5) $P_2$  (Fig. 6A); this prediction is corroborated by the experiments (Fig. 6B).

(2) We propose for the first time that the spatial distribution of the pacemaker site is in fact a key factor in determining the shape of the wave front. In particular, to reproduce the rather flat shape of the  $Ca^{2+}$  wave front observed in ascidian eggs, it is most appropriate to assume that the ER density varies only along the animal-vegetal axis. In the model, we have also assumed a higher ER density just below the plasma membrane to support the higher speed of propagation of the  $Ca^{2+}$  waves in the ascidian egg cortex. Such an assumption was also found to be necessary to reproduce the correct shape of the fertilization  $Ca^{2+}$  wave in frog eggs (Bugrim et al., 2003).

(3) Simulations highlight the fact that Ins(1,4,5) $P_3$  is not

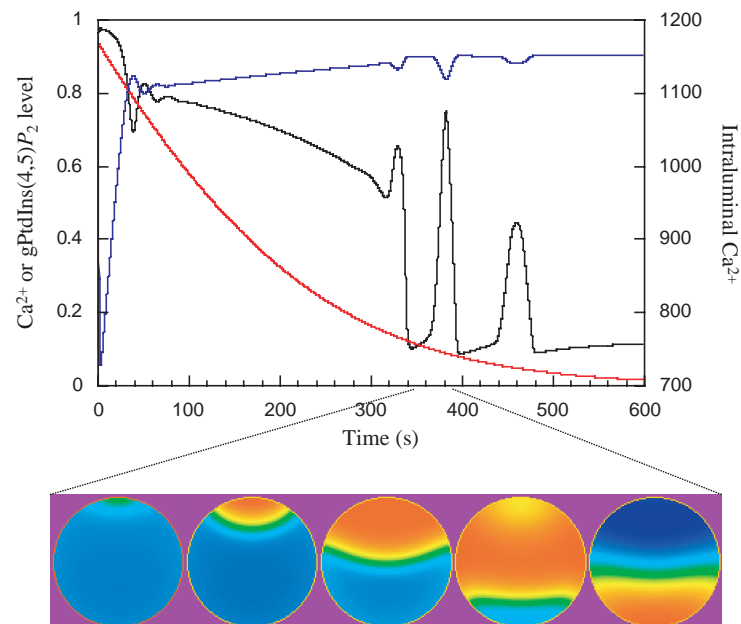


**Fig. 7.** Simulation of the effect of a massive, global increase of gIns(4,5) $P_2$  in the ascidian egg. The temporal pattern of the  $Ca^{2+}$  spike much resembles that observed at fertilization. Simulation has been performed as in Fig. 4 with  $I_{gPtdIns(4,5)P_2} = 25 \mu M \text{ second}^{-1}$  in the whole system during the flash time (0.3 seconds). The black, red and blue traces represent the average level of cytosolic  $Ca^{2+}$ , gPtdIns(4,5) $P_2$  and luminal  $Ca^{2+}$ , respectively.

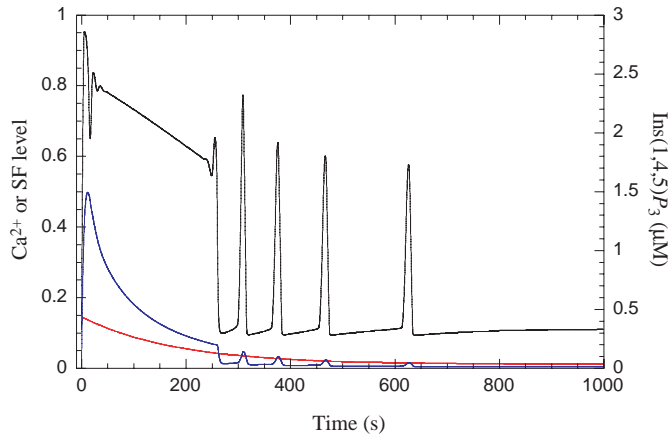


**Fig. 8.** Simulation of the series I  $\text{Ca}^{2+}$  oscillations induced by fertilization. Shown are the evolutions of the average concentrations in  $\text{Ca}^{2+}$  (black),  $\text{Ins}(1,4,5)\text{P}_3$  (blue) and SF (red). Results have been obtained by numerical simulations of equations (1), (4), (5') and (8) with the same parameter values as in Fig. 3. Moreover  $K_{\text{ASF}}=0.15 \mu\text{M}$ ,  $k_{\text{SF}}=5.56 \cdot 10^{-3} \text{ second}^{-1}$  and  $D_{\text{SF}}=150 \mu\text{m}^2 \text{ second}^{-1}$ . Initial conditions are the same as in Fig. 3, except that  $[\text{SF}]=50 \mu\text{M}$  in the mesh points (16 to 20) along the  $X$  and  $Y$  axes.

a global messenger in a cell as large as an ascidian egg and that it can have only a local action. In fact, this was already manifest in the experimental results showing that abortive  $\text{Ca}^{2+}$  waves are generally induced by localized flash photolysis of  $\text{Ins}(1,4,5)\text{P}_3$  [see Fig. 3A of Dumollard and Sardet (Dumollard and Sardet, 2001)]. In immature *Xenopus* oocytes, such abortive  $\text{Ca}^{2+}$  waves in response to localized  $\text{Ins}(1,4,5)\text{P}_3$  flashes have also been recorded (Marchant et al., 1999).

Significant variations in the  $\text{Ca}^{2+}$  content of the ER are predicted in the model only in the case of high amplitude and long-lasting cytosolic  $\text{Ca}^{2+}$  increases, such as those induced by a massive and global  $\text{gPtdIns}(4,5)\text{P}_2$  increase. Moreover, the initial level of  $\text{Ca}^{2+}$  in the ER greatly influences the shape and duration of these long lasting cytosolic  $\text{Ca}^{2+}$  increases, as it directly modulates the  $\text{Ins}(1,4,5)\text{P}_3$ -sensitive  $\text{Ca}^{2+}$  rise in the cytosol.

(4) In a second part of our study, we have used our model to investigate, in a theoretical manner, what could be the events upstream from  $\text{Ins}(1,4,5)\text{P}_3$  formation at fertilization. On the basis of the available data, we have made the assumption that the SF is a soluble factor like PLC (Swann et al., 2001). While the best candidate for the sperm factor in mammals is a new form of PLC ( $\text{PLC}\zeta$ ) (Saunders et al., 2002; Cox et al., 2002), the activity of the sperm factor of ascidians can be blocked by the injection of SH2 domains of  $\text{PLC}\gamma$  supposed to inhibit any  $\text{PLC}\gamma$  activity (Runft and Jaffe, 2000; Runft et al., 2002). It thus seems that the sperm factor of ascidians is a PLC or an activator of it.

Besides the experimental evidences in favour of the fact that the SF would be a PLC-like factor or its activator, we have ruled out the possibility that the SF in ascidians could be a molecule similar to  $\text{Ins}(1,4,5)\text{P}_3$ . We have indeed seen above [see section 'An artificial pacemaker site (PM3) is revealed by flash-photolysis of  $\text{Ins}(1,4,5)\text{P}_3$  or  $\text{gPtdIns}(4,5)\text{P}_2$ '] that  $\text{Ins}(1,4,5)\text{P}_3$  appears to be a local messenger that cannot, through a single increase, induce repetitive  $\text{Ca}^{2+}$  rises. By contrast, a theoretical study of the fertilization  $\text{Ca}^{2+}$  wave in

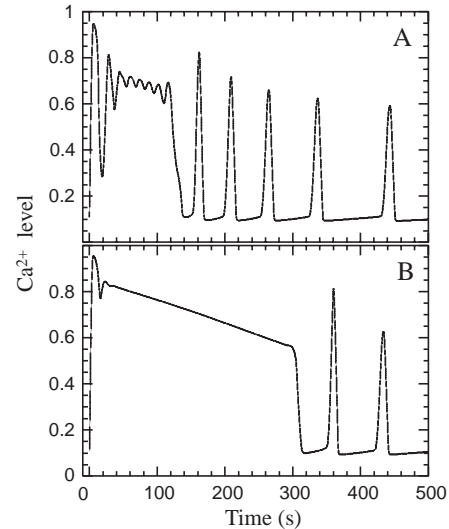


**Fig. 9.** Effect of varying the dose of SF injected into the egg. Simulations are the same as in Fig. 8, except for the initial localized rise in [SF], which equals  $35 \mu\text{M}$  for panel (A) and  $60 \mu\text{M}$  for panel (B).

*Xenopus* oocyte (Bugrim et al., 2003) concludes that an elevated concentration of  $\text{Ins}(1,4,5)\text{P}_3$  near the site of fertilization appears as the most probable mechanism to reproduce the experimental observations. The contradiction between the latter theoretical results and ours can be explained by the fact that the study for *Xenopus* oocytes simulates the unique fertilization wave as a switch between a stable state with low cytosolic  $\text{Ca}^{2+}$  and another stable state with a high cytosolic  $\text{Ca}^{2+}$ . The passage from one state to the other can, in this case, be induced by a sufficient perturbation, i.e. the initial localized rise in  $\text{Ins}(1,4,5)\text{P}_3$ . This hypothesis cannot hold for fertilization in ascidians or in mammals, where wave propagation must obviously be associated with an oscillatory (and not a bistable) dynamic.

The main conclusions that can be drawn from this second part of the study are summarized as follows.

(1) If the SF is a PLC, it must be  $\text{Ca}^{2+}$  sensitive. Otherwise, only spatially restricted  $\text{Ca}^{2+}$  waves would propagate when the level of SF becomes too low. The assumption of a  $\text{Ca}^{2+}$ -sensitive PLC appears crucial in the model to avoid the progressive decrease of the amplitude of the secondary  $\text{Ca}^{2+}$  spikes. In the case of a  $\text{Ca}^{2+}$ -insensitive PLC (not shown), the extent of the  $\text{Ca}^{2+}$  wave propagation decreases together with the level of  $\text{Ins}(1,4,5)\text{P}_3$ , which itself follows that of PLC activity. Thus, the amplitude of the  $\text{Ca}^{2+}$  spikes decreases with the level of PLC. This effect is also observed for  $\text{gPtdIns}(4,5)\text{P}_2$  injections (Fig. 7) and is the same as that observed and simulated with different doses of  $\text{Ins}(1,4,5)\text{P}_3$  (Fig. 3). By contrast, when PLC is stimulated by  $\text{Ca}^{2+}$ , a  $\text{Ca}^{2+}$  wave always invades the entire egg as the  $\text{Ca}^{2+}$  front itself generates the  $\text{Ins}(1,4,5)\text{P}_3$  required to propagate further. A recent study, published after we finished our simulations, reports that  $\text{PLC}\zeta$  is indeed  $\text{Ca}^{2+}$ -sensitive (Kouchi et al., 2004). Surprisingly, the characteristics of this  $\text{Ca}^{2+}$  activation quantitatively match our predictions; indeed it has been reported that the activation constant of  $\text{PLC}\zeta$  by  $\text{Ca}^{2+}$  lies

around  $10^{-7}$  M ( $K_{ASf}=0.15$   $\mu$ M in our model) and that this activation occurs cooperatively with a Hill coefficient of 1.7 [a value of 2 was put in equation (5')] (Kouchi et al., 2004). Conversely, our results would also agree with the other hypothesis that the SF in the ascidian could act via a PLC $\zeta$  (Runft and Jaffe, 2000; Runft et al., 2002), another  $Ca^{2+}$ -sensitive isoform of the PLC.

(2) The diffusibility of the SF must be rather high. In the model, we have assumed a diffusion coefficient of  $150$   $\mu$ m<sup>2</sup> second<sup>-1</sup>, which is higher than the value that would be predicted on the basis of the molecular mass of the PLC $\zeta$  [approximately 70 kDa (Cox et al., 2002)], which would correspond to a diffusion coefficient of about  $50$   $\mu$ m<sup>2</sup> second<sup>-1</sup>. However, our results have been obtained on the basis of an egg diameter of  $150$   $\mu$ m (corresponding to an ascidian egg), which is larger than that of a mouse egg (about  $70$   $\mu$ m), where the PLC $\zeta$  has been identified. In the ascidian egg, the molecular weight of the still-unknown sperm factor was estimated to lie in a range from 30 to 100 kDa (Kyojuka et al., 1998). This discordance might suggest that in ascidian eggs, the sperm factor is an activator of a  $Ca^{2+}$ -sensitive PLC, with a lower molecular weight than PLC itself.

(3) Further hypotheses have to be put forward to account for the observed relocalization of PM1. We have not yet simulated the possible movement of a source of SF. Simpler hypotheses, such as the existence of a region more sensitive to Ins(1,4,5) $P_3$  in the vegetal pole, or a preferential localization of the SF in this same region, have been tested in our model but did not lead to a good agreement with experimental results. We think, however, that the modelling of the movement of PM1 (and thereby the appearance of PM2) would be premature. Indeed, although the temporal  $Ca^{2+}$  patterns seen at fertilization or in response to massive gPtdIns(4,5) $P_2$  release are very similar, the spatial characteristics of both  $Ca^{2+}$  responses are different: in the case of gPtdIns(4,5) $P_2$  release, the second and successive  $Ca^{2+}$  waves emanate from PM3 in the animal pole; whereas in the case of fertilization, the initiation sites of the successive  $Ca^{2+}$  waves progressively relocate towards the vegetal pole. Thus, there is obviously a fertilization-related event (probably not mediated by  $Ca^{2+}$ ) that dictates the spatial characteristics of the late fertilization  $Ca^{2+}$  spikes triggered by PM1 and that needs to be better understood.

(4) The simulations shown here above all assume that the source of Ins(1,4,5) $P_3$ , i.e. PtdIns(4,5) $P_2$ , is present in the entire egg. This assumption was found to be necessary to allow correct propagation of the  $Ca^{2+}$  wave in the entire egg. If PtdIns(4,5) $P_2$  is assumed to be located only in the plasma membrane, the  $Ca^{2+}$  wave does not reach the centre of the egg and does not show the correct wave front. Again, this can be explained by the fact that Ins(1,4,5) $P_3$  is not a global messenger in a cell as large as an egg. From a physiological point of view, a plausible hypothesis would be that PtdIns(4,5) $P_2$  is, in fact, associated with intracellular organelles (Rice et al., 2000).

(5) Based on the results of our simulations, we propose that the temporal shape of the first large  $Ca^{2+}$  wave depends on the quantity of SF introduced into the egg. Thus, both the duration and the appearance of smaller amplitude  $Ca^{2+}$  spikes on the plateau phase can be modulated by the amount of SF supposed to be introduced into the egg (Fig. 9). Although such smaller-amplitude spikes on the plateau are not observed at the

fertilization of *Phallusia mammillata* (Dumollard and Sardet, 2001; Dumollard et al., 2002), they are clearly visible in other species such as *Ascidella aspersa* (Levasseur and McDougall, 1998; McDougall et al., 2000) or even in mammals (Swann et al., 2001). However, even though these additional spikes have been observed during the fertilization  $Ca^{2+}$  wave after natural fertilization, sperm extract or sperm factor RNA injections in *Ascidella* or mouse eggs, no correlation between the amount of sperm extract or sperm factor injection and the appearance of these spikes has yet been established.

In conclusion, our study demonstrates that when Ins(1,4,5) $P_3$  is produced throughout the whole ascidian egg, spatial inhomogeneities in the ER distribution are responsible for the appearance of the artificial  $Ca^{2+}$  wave pacemaker PM3 in the animal pole of the egg and dictates the spatio-temporal characteristics of the  $Ca^{2+}$  waves triggered by this pacemaker. This model also predicts that the activity of the natural pacemaker PM1 induced by fertilization is regulated by a soluble  $Ca^{2+}$ -activated PLC that is injected into the egg. This PLC should hydrolyse PtdIns(4,5) $P_2$  in the whole egg and its activity would oscillate leading to oscillatory changes in Ins(1,4,5) $P_3$  mediating PM1 function. This latter prediction can only be tested by monitoring the spatio-temporal variations of Ins(1,4,5) $P_3$  levels in a single egg undergoing fertilization. In the future, the model can be extended to investigate the origins of the detailed characteristics of the  $Ca^{2+}$  waves in the eggs of different species, for example, the periods of the waves, the existence of pacemaker zones other than those observed in ascidian eggs or the shapes of the  $Ca^{2+}$  spikes.

G.D. is 'Chercheur Qualifié du FNRS (Belgium)'. R.D. is a Marie Curie Fellow. We thank K. Swann, C. Sardet, A. McDougall and S. Swillens for critical reading of the manuscript.

## References

- Berridge, M. J., Lipp, P. and Bootman, M. D. (2000). The versatility and universality of calcium signalling. *Nat. Rev. Mol. Cell Biol.* **1**, 11-21.
- Bezprozvanny, I., Watras, J. and Ehrlich, B. (1991). Bell-shaped calcium responses of InsP<sub>3</sub>- and calcium-gated channels from endoplasmic reticulum of cerebellum. *Nature* **351**, 751-754.
- Bird, G., Obie, J. and Javie, J. (1992). Sustained  $Ca^{2+}$  signalling in mouse lacrimal acinar cells due to photolysis of caged glycerophosphoryl-myoinositol 4,5-bisphosphate. *J. Biol. Chem.* **267**, 17722-17725.
- Bugrim, A., Fontanilla, R., Eutenier, B., Keizer, J. and Nuccitelli, R. (2003). Sperm initiates a  $Ca^{2+}$  wave in frog eggs that is more similar to  $Ca^{2+}$  waves initiated by IP<sub>3</sub> than by  $Ca^{2+}$ . *Biophys. J.* **84**, 1580-1590.
- Carroll, M., Levasseur, M., Wood, C., Whitaker, M., Jones, K. and McDougall, A. (2003). Exploring the mechanism of action of the sperm-triggered calcium-wave pacemaker in ascidian zygotes. *J. Cell Sci.* **116**, 4997-5004.
- Cox, L., Larman, M., Saunders, C., Hashimoto, K., Swann, K. and Lai, F. (2002). Sperm phospholipase C $\zeta$  from humans and cynomolgus monkeys triggers  $Ca^{2+}$  oscillations, activation and development of mouse oocytes. *Reproduction* **124**, 611-623.
- Depierre, J. W. and Dallner, G. (1975). Structural aspects of the membrane of the endoplasmic reticulum. *Biochim. Biophys. Acta* **415**, 411-472.
- Dumollard, R. and Sardet, C. (2001). Three different calcium wave pacemakers in ascidian eggs. *J. Cell Sci.* **114**, 2471-2481.
- Dumollard, R., Carroll, J., Dupont, G. and Sardet, C. (2002). Calcium wave pacemakers in eggs. *J. Cell Sci.* **115**, 3557-3564.
- Dupont, G. (1998). Link between fertilization-induced  $Ca^{2+}$  oscillations and relief from metaphase II arrest in mammalian eggs: a model based on calmodulin-dependent kinase II activation. *Biophys. Chem.* **72**, 153-167.
- Dupont, G. and Erneux, C. (1997). Simulations of the effect of inositol 1,4,5-trisphosphate 3-kinase and 5-phosphatase activities on  $Ca^{2+}$  oscillations. *Cell Calcium* **22**, 321-331.

- Dupont, G. and Swillens, S. (1996). Quantal release, incremental detection, and long-period oscillations in a model based on regulatory  $\text{Ca}^{2+}$ -binding sites along the permeation pathway. *Biophys. J.* **71**, 1714-1722.
- Dupont, G., Tordjmann, T., Clair, C., Swillens, S., Claret, M. and Combettes, L. (2000). Mechanism of receptor-oriented intercellular calcium wave propagation in hepatocytes. *FASEB J.* **14**, 279-289.
- Finch, E., Turner, T. and Golden, S. (1991). Calcium as coagonist of inositol 1,4,5-trisphosphate-induced calcium release. *Science* **252**, 443-446.
- Fink, C., Slepchenko, B., Moraru, I., Watras, J., Schaff, J. and Loew, L. (2000). An image-based model of calcium waves in differentiated neuroblastoma cells. *Biophys. J.* **79**, 163-183.
- Fontanilla, R. and Nuccitelli, R. (1998). Characterization of the sperm-induced calcium wave in *Xenopus* eggs using confocal microscopy. *Biophys. J.* **75**, 2079-2087.
- Goldbeter, A. (1996). *Biochemical oscillations and cellular rhythms*. Cambridge, UK: Cambridge University Press.
- Goldbeter, A., Dupont, G. and Berridge, M. J. (1990). Minimal model for signal-induced  $\text{Ca}^{2+}$  oscillations and for their frequency encoding through protein phosphorylation. *Proc. Natl. Acad. Sci. USA* **87**, 1461-1465.
- Hirose, K., Kadowski, S., Tanabe, M., Takeshima, H. and Iino, M. (1999). Spatio-temporal dynamics of inositol 1,4,5-trisphosphate that underlies complex  $\text{Ca}^{2+}$  mobilization patterns. *Science* **284**, 1527-1530.
- Hofer, A. and Schulz, I. (1996). Quantification of intraluminal free [Ca] in the agonist-sensitive internal calcium store using compartmentalized fluorescent indicators: some considerations. *Cell. Calcium* **20**, 235-242.
- Howell, K., Skipwith, A., Galione, A. and Eckberg, W. (2003). Phospholipase C-dependent  $\text{Ca}^{2+}$  release by worm and mammal sperm factors. *Biochem. Biophys. Res. Commun.* **307**, 47-51.
- Hunding, A. and Ipsen, M. (2003). Simulation of waves in calcium models with 3D spherical geometry. *Math. Biosci.* **182**, 45-66.
- Kouchi, Z., Fukami, K., Shikano, T., Oda, S., Nakamura, Y., Takenawa, T. and Miyazaki, S. (2004). Recombinant phospholipase  $\text{C}\zeta$  has high  $\text{Ca}^{2+}$ -sensitivity and induces  $\text{Ca}^{2+}$  oscillations in mouse eggs. *J. Biol. Chem.* **279**, 10408-10412.
- Kurokawa, M., Sato, K. and Fissore, R. (2004). Mammalian fertilization: from sperm factor to phospholipase  $\text{C}\zeta$ . *Biol. Cell* **96**, 37-46.
- Kyozuka, K., Deguchi, R., Mohri, T. and Miyazaki, S. (1998). Injection of sperm extract mimics spatiotemporal dynamics of  $\text{Ca}^{2+}$  responses and progression of meiosis at fertilization of ascidian oocytes. *Development* **125**, 4099-4105.
- Lechleiter, J., Girard, S., Peralta, E. and Clapham, D. (1991). Spiral calcium wave propagation and annihilation in *Xenopus laevis* oocytes. *Science* **252**, 123-126.
- Levasseur, M. and McDougall, A. (2000). Sperm-induced calcium oscillations at fertilisation in ascidians are controlled by cyclin B1-dependent kinase activity. *Development* **127**, 631-641.
- Marchant, J., Callamaras, N. and Parker, I. (1999). Initiation of  $\text{InsP}_3$ -mediated  $\text{Ca}^{2+}$  waves in *Xenopus* oocytes. *EMBO J.* **18**, 5285-5299.
- McDougall, A. and Sardet, C. (1995). Function and characteristics of repetitive calcium waves associated with meiosis. *Curr. Biol.* **5**, 318-328.
- McDougall, A., Levasseur, M., O'Sullivan, A. and Jones, K. (2000). Cell cycle-dependent  $\text{Ca}^{2+}$  waves induced by a cytosolic sperm extract in mature ascidian oocytes mimic those observed at fertilization. *J. Cell Sci.* **113**, 3453-3462.
- Meyer, T. and Stryer, L. (1988). Molecular model for receptor-stimulated calcium spiking. *Proc. Natl. Acad. Sci. USA* **85**, 5051-5055.
- Miyakawa, T., Maeda, A., Yamazawa, T., Hirose, K., Kurosaki, T. and Iino, M. (1999). Encoding of  $\text{Ca}^{2+}$  signals by differential expression of  $\text{InsP}_3$  receptor subtypes. *EMBO J.* **18**, 1303-1308.
- Montero, M., Brini, M., Marsault, R., Alvarez, J., Sitia, R., Pozzan, T. and Rizzuto, R. (1995). Monitoring dynamic changes in free  $\text{Ca}^{2+}$  concentration in the endoplasmic reticulum of intact cells. *EMBO J.* **14**, 5467-5475.
- Ozil, J.-P. (1998). Role of calcium oscillations in mammalian egg activation: experimental approach. *Biophys. Chem.* **72**, 141-152.
- Renard, D., Poggioli, J., Berthon, B. and Claret, M. (1987). How far does phospholipase C depend on the cell calcium concentration? *Biochem. J.* **243**, 391-398.
- Rhee, S. and Choi, K. (1992). Multiple forms of phospholipase C isozymes and their activation mechanisms. *Adv. Second Messenger Phosphoprotein Res.* **26**, 35-61.
- Rice, A., Parrington, J., Jones, K. and Swann, K. (2000). Mammalian sperm contain a  $\text{Ca}^{2+}$ -sensitive phospholipase C activity that can generate  $\text{InsP}_3$  from  $\text{PIP}_2$  associated with intracellular organelles. *Dev. Biol.* **228**, 125-135.
- Roegiers, F., Djediat, C., Dumollard, R., Rouviere, C. and Sardet, C. (1999). Phases of cytoplasmic and cortical reorganizations of the ascidian zygote between fertilisation and first division. *Development* **126**, 3101-3117.
- Runft, L. and Jaffe, L. A. (2000). Sperm extract injection into ascidian eggs signals  $\text{Ca}^{2+}$  release by the same pathway as fertilization. *Development* **127**, 3227-3236.
- Runft, L., Jaffe, L. and Mehlmann, L. (2002). Egg activation at fertilization: where it all begins. *Dev. Biol.* **15**, 237-254.
- Sardet, C., Prodon, F., Dumollard, R., Chang, P. and Chenevert, J. (2002). Structure and function of the egg cortex from oogenesis through fertilization. *Dev. Biol.* **241**, 1-23.
- Saunders, C., Larman, M., Parrington, J., Cox, L., Royse, J., Blayney, L., Swann, K. and Lai, F. (2002).  $\text{PLC}\zeta$ : a sperm-specific trigger of  $\text{Ca}^{2+}$  oscillations in eggs and embryo development. *Development* **129**, 3533-3544.
- Schuster, S., Marhl, M. and Höfer, T. (2002). Modelling of simple and complex calcium oscillations. *Eur. J. Biochem.* **269**, 1333-1355.
- Sims, C. and Allbritton, N. (1998). Metabolism of inositol 1,4,5-trisphosphate and inositol 1,3,4,5-tetrakisphosphate by the oocytes of *Xenopus laevis*. *J. Biol. Chem.* **273**, 4052-4058.
- Sneyd, J., Keizer, J. and Sanderson, M. (1995). Mechanisms of calcium oscillations and waves: a quantitative analysis. *FASEB J.* **9**, 1463-1472.
- Speksnijder, J., Corson, D. and Jaffe, L. (1989). Free calcium pulses following fertilization in the ascidian egg. *Dev. Biol.* **135**, 182-190.
- Stricker, S. (1999). Comparative biology of calcium signalling during fertilization and egg activation in animals. *Dev. Biol.* **211**, 157-176.
- Swann, K. (1996). Soluble sperm factors and  $\text{Ca}^{2+}$  release in eggs at fertilization. *Rev. Reprod.* **1**, 33-39.
- Swann, K. and Parrington, J. (1999). Mechanism of  $\text{Ca}^{2+}$  release at fertilization in mammals. *J. Exp. Zool.* **15**, 267-275.
- Swann, K., Parrington, J. and Jones, K. (2001). Potential role of a sperm-derived phospholipase C in triggering the egg-activating  $\text{Ca}^{2+}$  signal at fertilization. *Reproduction* **122**, 839-847.
- Wagner, J., Li, Y.-X., Pearson, J. and Keizer, J. (1998). Simulation of the fertilization  $\text{Ca}^{2+}$  wave in *Xenopus laevis* eggs. *Biophys. J.* **75**, 2088-2097.
- Xu, C., Watras, J. and Loew, L. (2003). Kinetic analysis of receptor-activated phosphoinositide turnover. *J. Cell Biol.* **161**, 779-791.